

Band Offsets in Heterojunctions Formed by Oxides with Cubic Perovskite Structure

A. I. Lebedev

Moscow State University, Moscow, 119991 Russia

e-mail: swan@scon155.phys.msu.ru

Received November 11, 2013

Abstract—A number of recent discoveries on heterostructures formed by oxides suggest the emergence of a new direction in microelectronics, the oxide electronics. In the present work, band offsets in nine heterojunctions formed by titanates, zirconates, and niobates with the cubic perovskite structure are calculated from first principles. The effect of strain in contacting oxides on their energy structure; the GW corrections to the band edge positions resulting from many-body effects; and the conduction band edge splitting resulting from spin-orbit coupling are consistently taken into account. It is shown that the neglect of the many-body effects can cause errors in the determination of the band offsets, reaching 0.36 eV. The fundamental inapplicability of the transitivity rule often used to determine the band offsets in heterojunctions by comparing the band offsets in a pair of heterojunctions formed by the components of the heterojunction under study with a third common component is demonstrated. The cause of the inapplicability is explained.

DOI: 10.1134/S106378341405014X

1. INTRODUCTION

Almost all electronic and optoelectronic devices contain metal–semiconductor, metal–dielectric, semiconductor–ferroelectric, or semiconductor–semiconductor interfaces. Since the electron energy changes abruptly at the interface, the characteristics of devices containing such interfaces directly depend on the heights of emerging energy barriers. Although the concept of a heterojunction was first introduced for the contact of two semiconductors, its use is currently significantly extended and includes dielectrics. For example, in solving the important problem of the substitution of the SiO_2 gate dielectric in silicon field-effect transistors with a material with a higher dielectric constant, the calculation of the tunneling current through the gate dielectric requires an accurate knowledge of the energy band diagram of the formed heterojunction.

In the last decade, experimental studies have discovered a number of new physical phenomena occurring at the interface of two oxide dielectrics: the formation of a quasi-two-dimensional electron gas at the heterointerface [1]; the appearance of magnetism at the interface of two non-magnetic oxides [2]; the superconductivity of the quasi-two-dimensional electron gas [3], and the possibility of controlling the superconducting transition temperature by an electric field [4]. In experiments [5, 6], the possibility of controlling the conductivity in a quasi-two-dimensional layer by an electric field was demonstrated (an analogue of the field effect). The strongest effect was observed if a ferroelectric was used as one of oxides [7].

When the heterostructure components were magnetic and ferroelectric oxides, it was possible to control the magnetic properties of a magnet and the magnetoresistive effect observed in it by a switchable ferroelectric polarization [8–10]. Thus, these heterostructures acquired the properties of multiferroics. The above-mentioned and other new phenomena discovered in oxide heterostructures form a basis for developing new multifunctional electronic devices and suggest the emergence of a new direction in microelectronics, the oxide electronics [11–13].

One of the applications of ferroelectric oxides is the ferroelectric memory. The development of such devices requires solving the problems of nondestructive information read-out and the increase in the packing density of memory cells. When using nondestructive optical read-out methods, the cell sizes are limited by the used wavelength. The typical band gap of titanates with the perovskite structure is ~ 3 eV; therefore, the minimum cell size is ~ 0.4 μm . When using multiferroics, in which the information is stored electrically and read out magnetically, the cell sizes can be decreased to sizes typical of modern hard disks, i.e., ~ 500 Å (when using homogeneous multiferroic thin films, the physical size of the memory cells is limited by a rather large thickness of the magnetic domain wall).

The methods based on electrical read-out of the ferroelectric polarization seem the most promising. For example, the nonlinear current–voltage characteristics reversible upon switching the polarization direction, which were recently observed in metal–fer-

roelectric–metal structures formed on single crystals and thin films of BiFeO_3 [14, 15], can be used for non-destructive information read-out from the memory cells. Structures that use the tunneling through an ultrathin ferroelectric layer can find similar application [16–18]. Since the physical limit of the memory cell size in the ferroelectric memory with electrical read-out is the ferroelectric domain wall thickness and the minimum film thickness at which the ferroelectricity still exists (both sizes are a few unit cells [19–22]), the packing density in such memory devices will be maximum.

The most important physical parameters characterizing an interface between two semiconductors or dielectrics are the band offsets in the energy band diagram of a heterojunction. The valence band offset ΔE_v (the conduction band offset ΔE_c) is defined as the difference between the positions of the tops of the valence bands (bottoms of the conduction bands) in two contacting materials. These band offsets control many physical properties of heterojunctions, in particular, their electrical and optical properties.

For oxides with the perovskite structure there are experimental data on the band offsets for perovskite/Si [23, 24], $\text{SrTiO}_3/\text{SrO}$ and $\text{BaTiO}_3/\text{BaO}$ heterojunctions [25], but the data for heterojunctions formed by two perovskite dielectrics are very limited [26–29]. In addition, there are data on the Schottky barrier heights for perovskite–metal structures in which Pt, Au, Ag, and conductive SrRuO_3 and $(\text{La}, \text{Sr})\text{CoO}_3$ oxides are used as a metal.

In this work, the band offsets in heterojunctions formed by titanates, zirconates, and niobates with the cubic perovskite structure are calculated from first principles using the density functional theory and GW approximation. The obtained results are compared with available experimental data.

2. CALCULATION METHODOLOGY

The band offsets cannot be determined by simple comparison of corresponding band edge energies obtained in independent first-principles calculations of the band structure of two bulk materials. This is due to the absence of intrinsic energy scale in such calculations: the energies corresponding to the valence band edge E_v and the conduction band edge E_c are usually measured from an average of the electrostatic potential which is a poorly defined quantity in infinite systems. Therefore, in addition to calculations of the band structure of two contacting materials, the change in the average of the electrostatic potential ΔV at the interface of two materials should also be calculated. This quantity is determined by the dipole moment emerging at the heterointerface due to the electron density redistribution at hybridized orbitals in contacting materials, and accounts for all features inher-

ent to the interface, such as variations of chemical composition, structure distortions, and so on.

Thus, the band offset in the valence band can be written as a sum of two terms [30]

$$\Delta E_v = (E_{v2} - E_{v1}) + \Delta V. \quad (1)$$

The first term in this formula is the difference of energies corresponding to the tops of the valence bands, which are determined from standard band-structure calculations of bulk materials. The second term is the change of the average of the electrostatic potential through the heterojunction.

To calculate ΔV , one usually starts from the total potential (the potential of ions plus the microscopic electrostatic Hartree potential for electrons) obtained from the self-consistent electron density calculation in the superlattice constructed of the contacting materials. Then the macroscopic averaging technique [31] is used, in which the electrostatic potential is first averaged over planes parallel to the interface, and then the obtained quasi-periodic one-dimensional function is convoluted with two rectangular filters whose lengths are determined by the periods of components. The obtained profiles of the average electrostatic potential $\bar{V}(r)$ contain flat (bulk-like) regions sufficiently far from the heterojunction. The quantity ΔV is defined as the energy difference between these plateaus. It should be noted that neither the quantities E_{v1} and E_{v2} themselves nor ΔV have physical meaning; only their sum (1) is physically meaningful.

The offset in the conduction band is calculated from ΔE_v and the difference of band gaps in two materials,

$$\Delta E_c = (E_{c2} - E_{c1}) + \Delta V = (E_{g2} - E_{g1}) + \Delta E_v.$$

The band gap $E_g = E_c - E_v$ can be roughly estimated in the LDA approximation for the exchange-correlation energy. However, because of the well-known band gap problem characteristic of this one-electron approach, more accurate calculations require to take into account the corrections to the band edges positions resulting from many-body effects. These corrections to the self-energy (ΔE_c^{QP} and ΔE_v^{QP}) are usually calculated within the quasiparticle GW approximation. It is usually believed that many-body corrections adjust the conduction band position, thus solving the band gap problem; however, the energy levels in the valence band become also subjected to the correction.

In the case of well-studied materials, ΔE_c is often calculated using experimental band gaps. However, if the band offset ΔE_v was obtained theoretically, the problem associated with the uncertainty in ΔE_v^{QP} remains. It is often assumed that the ΔE_v^{QP} values in two materials are close, so that their contributions

cancel each other. In this work, it will be shown that in the general case this assumption is not true.

It should also be kept in mind that E_{v1} , E_{c1} , E_{v2} , and E_{c2} should be calculated at the same materials strains as in the heterojunction itself, since the energy levels in a crystal depend on interatomic distances. In this case, in addition to possible splitting of degenerate levels corresponding to the band edges, the band gap can also vary. Moreover, the calculations should take into account the possible lifting of the band edge degeneracy resulting from spin–orbit coupling. Although such physical properties of dielectrics as lattice parameters and equilibrium positions of atoms depend weakly on spin–orbit coupling (that is why spin–orbit coupling is usually neglected in calculating these values), spin–orbit coupling significantly affects the energy position of band edges and the band gap, and it cannot be neglected in the band-structure calculations. The spin–orbit coupling effects in dielectrics can be considered a posteriori, i.e., after completing the main first-principles calculations.

3. CALCULATION TECHNIQUE

The objects of the present calculations were heterojunctions formed by titanates and zirconates of calcium, strontium, barium, and lead, and the $\text{KNbO}_3/\text{NaNbO}_3$ heterojunction. The heterojunctions were modeled using superlattices grown in the [001] direction and constructed of two materials with equal thickness of layers, each of four perovskite unit cells. The in-plane lattice parameter was determined from the condition of zero strain in the layers plane (i.e., it was close to the lattice parameter of the solid solution with the component ratio of 1:1). The atomic displacements normal to the interface were completely relaxed and the superlattice period was determined in the zero-strain condition in this direction.

The equilibrium lattice parameters and atomic coordinates in the superlattices were calculated from first principles within the density functional theory using the ABINIT software. The exchange–correlation interaction was described in the local density approximation (LDA). Atomic pseudopotentials were taken from [32, 33]. The maximum plane-wave energy was 30 Ha (816 eV). Integration over the Brillouin zone was performed using the $8 \times 8 \times 2$ Monkhorst–Pack mesh. All calculations were performed for heterojunctions formed by cubic $Pm3m$ phases; the effect of the possible polar and structural distortions of materials on the band offsets will be considered elsewhere. The value of ΔV was determined using the macroscopic averaging technique [31]. The values of E_{v1} , E_{c1} , E_{v2} , and E_{c2} in contacting materials were obtained from similar calculations for isolated crystals with the in-plane lattice parameter equal to the lattice parameter of the superlattice under study; in the third dimension, crystals were considered to be stress-free.

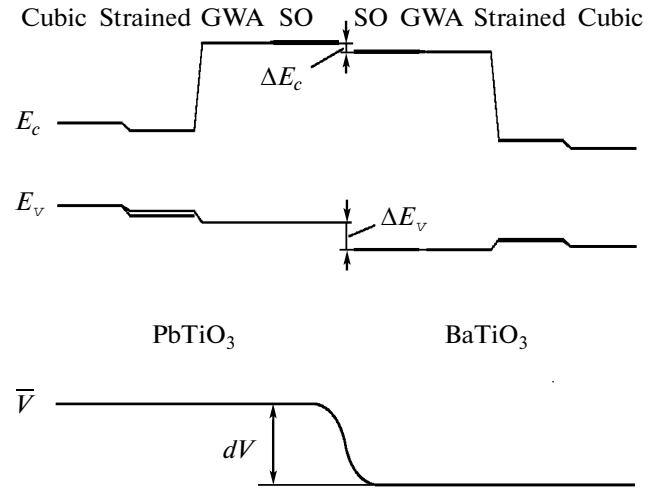


Fig. 1. Steps of the band offsets calculation in heterojunctions. First, changes in the band structure of cubic phases caused by strain in the heterojunction are taken into account; then, corrections for many-body effects (GWA) and finally the band splitting caused by spin–orbit (SO) coupling are considered. The lower diagram shows the change through the heterojunction of the average of the electrostatic potential from which all energy levels are measured.

The quasiparticle band gap and the many-body corrections to the band edge positions were calculated in the one-shot GW approximation [34].¹ The Kohn–Sham wave functions and energies calculated using the density functional theory in the LDA approximation were used as the zeroth-order approximation. The dielectric matrix $\epsilon_{GG'}(\mathbf{q}, \omega)$ was calculated for the $6 \times 6 \times 6$ mesh of wave vectors \mathbf{q} from the irreducible polarizability matrix $P_{GG'}^0(\mathbf{q}, \omega)$ calculated for 2200–2800 vectors $\mathbf{G}(\mathbf{G}')$ in reciprocal space, 20–22 filled and 278–280 empty bands. Dynamic screening was described in the Godby–Needs plasmon-pole model. Wave functions with energies up to 24 Ha were taken into account in the calculations. The energy corrections to the LDA solution were calculated from the diagonal matrix elements of the $[\Sigma - E_{xc}]$ operator, where $\Sigma = GW$ is the self-energy operator (the mass operator), E_{xc} is the exchange–correlation energy operator, G is the Green’s function, and $W = \epsilon^{-1}v$ is the screened Coulomb interaction. In the calculation of Σ , the wave functions with energies up to 24 Ha were taken into account.

4. RESULTS

Figure 1 shows the steps of the heterojunction energy band diagram calculation. The leftmost and rightmost diagrams in the figure relate to individual

¹ The results of these calculations will be described elsewhere in more detail.

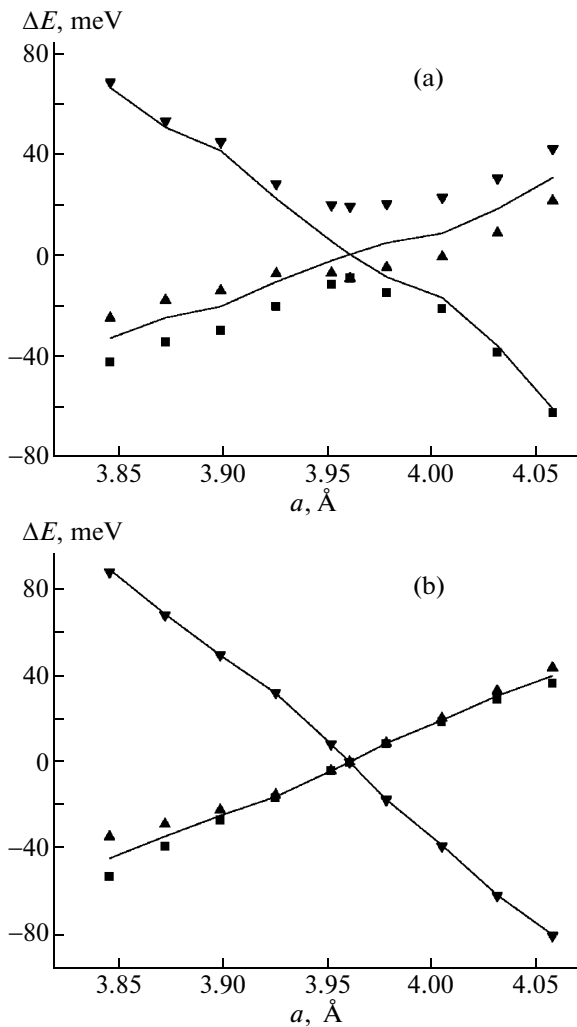


Fig. 2. Effect of biaxial strain of cubic BaTiO_3 on the (a) conduction and (b) valence band edges splitting without (curves) and with (dots) taking into account spin-orbit coupling. The calculated lattice parameter of the stress-free crystal is 3.962 \AA .

compounds with the cubic $Pm3m$ structure whose lattice parameters correspond to zero external stress. The biaxial strain of these materials during formation of a heterojunction, when their in-plane lattice parameters become equal, reduces the symmetry of their unit cells to $P4/mmm$. As a result, the band gaps of the materials are changed and the degeneracy at some points of the Brillouin zone is lifted. For example, the threefold degeneracy of the conduction band at the Γ point and that of the valence band at the R point are lifted (Fig. 2). These positions of extrema at the Γ and R points are characteristic of all compounds considered in this work, except for PbTiO_3 and PbZrO_3 . In cubic PbTiO_3 , the valence band extremum is at the X point, and the tetragonal distortion removes the valley degeneracy (depending on the strain sign, the valence band edge extremum is located either at the X point or

at the Z point of the Brillouin zone of the tetragonal lattice). In cubic PbZrO_3 , the only compound in which both band extrema are at the X point, the strain also removes the valley degeneracy, but both extrema remain at the same point of the Brillouin zone (X or Z). The energy diagrams of strained crystals are shown in Fig. 1 near the diagrams of initial cubic phases. We note that not only the band gap, but also the energy positions of the E_c and E_v band edges measured from the average of the electrostatic potential are changed upon strain. These energies in strained crystals are given in Tables 1 and 2.

The calculation of the corrections to the positions of the valence band edge ΔE_v^{QP} and the conduction band edge ΔE_c^{QP} within the GW approximation shows that the many-body effects shift the conduction band edge upward in energy by $\sim 1.3 \text{ eV}$ in all compounds considered in this work, except for PbZrO_3 in which the shift is only 0.266 eV (Tables 1 and 2). The valence band corrected for many-body effects shifts downward by $0.22\text{--}0.58 \text{ eV}$. Although the absolute values of the shifts under consideration slowly converge with increasing number of empty bands taken into account in the GW calculations (see, e.g., [35]), the relative drift of the difference between these shifts in different compounds is small. Therefore, if the same total number of bands (300 in our calculations) is used in the calculations of the corrections, the error in the determination of the relative position of band edges in two materials will be small, $\sim 0.01 \text{ eV}$ according to our estimates. Moreover, in our calculations it was assumed that the many-body corrections depend weakly on strain-induced structure distortions, and the values calculated for cubic crystals were used. The tests have shown that additional strain-induced changes of ΔE_v^{QP} and ΔE_c^{QP} can reach $0.01\text{--}0.02 \text{ eV}$, which provides some insight into possible errors. The energy diagrams of contacting materials after taking into account many-body effects are also shown in Fig. 1.

The calculations of many-body corrections show that the assumption used by many authors about an approximate equality of these corrections in two contacting materials is not valid in the general case. It is seen that the spread in the ΔE_v^{QP} values reaches 0.36 eV in related oxides with the cubic perovskite structure. This value is a measure of the possible error in the determination of the band offsets in calculations that neglect the many-body effects.²

Since our crystals contain atoms with high enough nucleus charge, the errors in the determination of the band edges positions resulting from the neglect of

² More detailed studies show that in a wide class of oxides, fluorides, and nitrides the ΔE_v^{QP} variation range reaches 3 eV . These results and their explanation will be published elsewhere.

Table 1. Parameters determining the valence band offset ΔE_v in the energy band diagram of studied heterojunctions (all energies are in eV)

Heterojunction	E_{v2}	ΔE_{v2}^{QP}	E_{v1}	ΔE_{v1}^{QP}	ΔV	ΔE_v
SrTiO ₃ /PbTiO ₃	13.629	-0.239	15.464	-0.315	+2.143	+0.384
BaTiO ₃ /BaZrO ₃	13.422	-0.512	13.766	-0.226	+0.066	-0.564
PbTiO ₃ /PbZrO ₃	12.390	-0.321	13.123	-0.239	+0.495	-0.320
PbTiO ₃ /BaTiO ₃	14.291	-0.226	13.453	-0.239	-1.276	-0.425
SrTiO ₃ /BaTiO ₃	14.366	-0.226	15.333	-0.315	+0.864	-0.014
SrTiO ₃ /SrZrO ₃	14.391	-0.582	14.912	-0.315	+0.395	-0.393
PbZrO ₃ /BaZrO ₃	13.158	-0.512	11.888	-0.321	-1.209	-0.130
SrTiO ₃ /CaTiO ₃	15.631	-0.333	15.664	-0.315	+0.131	+0.080
KNbO ₃ /NaNbO ₃	13.617	-0.314	14.494	-0.245	+0.944	-0.002

Table 2. Parameters determining the conduction band offset ΔE_c in the energy band diagram of heterojunctions and their types (all energies are in eV)

Heterojunction	E_{c2}	ΔE_{c2}^{QP}	ΔE_{c2}^{SO}	E_{c1}	ΔE_{c1}^{QP}	ΔE_{c1}^{SO}	ΔE_c	Type
SrTiO ₃ /PbTiO ₃	14.899	+1.326	-0.010	17.034	+1.431	-0.007	-0.100	I
BaTiO ₃ /BaZrO ₃	16.363	+1.199	-0.026	15.143	+1.341	-0.008	+1.126	I
PbTiO ₃ /PbZrO ₃	14.513	+0.266	0	14.269	+1.326	-0.010	-0.311	II
PbTiO ₃ /BaTiO ₃	15.820	+1.341	-0.008	14.704	+1.326	-0.010	-0.143	II
SrTiO ₃ /BaTiO ₃	15.885	+1.341	-0.008	16.879	+1.431	-0.007	-0.221	II
SrTiO ₃ /SrZrO ₃	17.469	+1.283	-0.023	16.347	+1.431	-0.007	+1.353	I
PbZrO ₃ /BaZrO ₃	16.116	+1.199	-0.026	14.069	+0.266	0	+1.745	I
SrTiO ₃ /CaTiO ₃	17.207	+1.486	-0.007	17.237	+1.431	-0.007	+0.156	II
KNbO ₃ /NaNbO ₃	15.005	+1.008	-0.038	15.823	+0.976	-0.037	+0.157	I

Table 3. Spin-orbit splittings of states at the Γ point of the conduction band in cubic perovskites (in meV)

CaTiO ₃	SrTiO ₃	BaTiO ₃	PbTiO ₃	SrZrO ₃	BaZrO ₃	NaNbO ₃	KNbO ₃
20.7	22.0	25.3	28.5	70.2	77.5	113.7	111.0

spin-orbit coupling can be rather large. In this work, the spin-orbit splitting Δ_{SO} of the valence and conduction band edges was calculated using the fully relativistic pseudopotentials [36]. The tests performed for a number of semiconductors (Ge, GaAs, CdTe), for which the spin-orbit splitting of the valence band is accurately determined experimentally, showed that the results of these calculations agree with experiment with an accuracy of $\sim 5\%$.

Calculations show that the spin-orbit coupling results in the band edge splitting at certain points of the Brillouin zone. First of all, this is true for the conduction band edge at the Γ point. It is interesting that, despite the presence of such heavy atoms as Ba and Pb in our crystals, the spin-orbit splitting is not so large. This is because the conduction band states at the Γ

point in the perovskite structure are mostly formed of d -states of the B atom (Ti, Zr, Nb). The spin-orbit splittings Δ_{SO} of the conduction band edge at the Γ point for all studied materials except for PbZrO₃ are given in Table 3. In PbZrO₃, the conduction band minimum is at the X point, it is non-degenerate, and is not subjected to spin-orbit splitting. The valence band edge (at R and X points) in all cubic crystals studied in this work is not split if the spin-orbit coupling is taken into account.

Since the centroid of the energy levels split by spin-orbit coupling coincides with the level position calculated without spin-orbit coupling [37] and the spin-orbit split-off conduction band at the Γ point is always shifted to higher energies in all studied crystals, the conduction band minimum at the Γ point appears

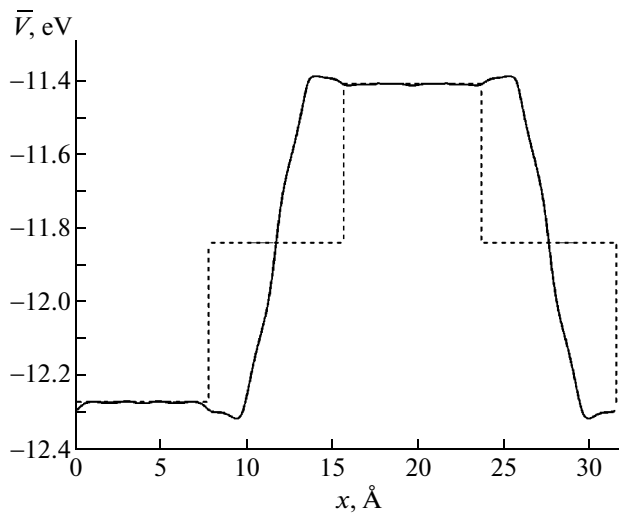


Fig. 3. Determination of ΔV from the profile of the average of the electrostatic potential $\bar{V}(x)$ for the SrTiO₃/BaTiO₃ superlattice (solid curve). The dashed curve is the approximating function.

shifted downward by $\Delta_{SO}/3$. This value determines an additional shift of the conduction band edge and is given in Table 2. The final energy band diagram of the heterojunction obtained after taking into account the spin-orbit coupling is shown by two internal diagrams in Fig. 1. We note that in these calculations we neglected the weaker effects associated with changes in the band splitting resulting from the strain-induced mixing of the spin-orbit split states, which can be seen in Fig. 2. These effects do not exceed 10 meV and are smaller than other systematic errors in our calculations.

In calculating ΔV , the averaged electrostatic potential profile $\bar{V}(r)$ obtained using the macroscopic averaging technique was approximated by a step function with transition regions of one lattice parameter (Fig. 3). The tests showed that when the individual layer thickness in the BaTiO₃/SrTiO₃ superlattice was changed from three to five unit cells, the variation of ΔV calculated using the described algorithm was only ~ 4 meV; this makes an estimate of the error in the ΔV determination. As shown in [38], the many-body effects have a weak influence on ΔV .

The results of the band offsets calculation for nine heterojunctions are given in Tables 1 and 2. The signs of the band offsets are defined as the energy change in going from the compound indicated the first in the heterojunction pair to the compound indicated the second. Depending on the energy band diagram, the heterojunctions are classified as type-I, for which the signs of ΔE_c and ΔE_v are opposite, and type-II, for which the signs of ΔE_c and ΔE_v are identical. The types of the heterojunctions are given in Table 2 and their energy band diagrams are shown in Fig. 4.

5. DISCUSSION

Unfortunately, the experimental data on the band offsets in heterojunctions between oxides with the perovskite structure is very limited. In [27], the band offsets in the SrTiO₃/SrZrO₃ heterojunction were studied by photoelectron spectroscopy. According to the measurements, this heterojunction is type I, and the band offsets are $\Delta E_v = -0.5 \pm 0.15$ eV and $\Delta E_c = +1.9 \pm 0.15$ eV (the top of the valence band in SrTiO₃ is higher than that in SrZrO₃). The data of the present calculations are in good agreement with these experimental data: according to our data, the heterojunction is also type I; the band offsets are -0.393 and $+1.353$ eV, respectively. In our opinion, the cause of a large discrepancy between the experimental and calculated values of ΔE_c is the fact that SrZrO₃ at 300 K has a distorted (orthorhombic) structure in which the band gap is larger than in the cubic phase. One more cause of disagreement can be the fact that the structures [27] were grown on SrTiO₃ substrates; hence, the calculated band offsets, which depend on the in-plane lattice parameter, can be slightly different (this dependence is well known for semiconductor heterojunctions [30, 37, 39]). To test the possible changes, the calculations were repeated for the SrTiO₃/SrZrO₃ heterojunction with the in-plane lattice parameter equal to the lattice parameter of SrTiO₃; these calculations yielded $\Delta E_v = -0.240$ eV and $\Delta E_c = +1.230$ eV, which slightly worsened the agreement with experiment.

The experimental data for the SrTiO₃/PbTiO₃ heterojunction [26] differ appreciably from the results of our calculations. According to the photoelectron spectroscopy data, it is a type-II heterojunction, and the band offsets are $\Delta E_v = +1.1 \pm 0.1$ eV and $\Delta E_c = +1.3 \pm 0.1$ eV (the top of the valence band in PbTiO₃ is higher than in SrTiO₃). According to our calculations, the band offsets are $+0.384$ and -0.100 eV, respectively, and the heterojunction is type I. Thus, the signs of ΔE_v in the calculations and experiment are identical, but the values themselves differ appreciably. The fact that at 300 K the crystal structure of PbTiO₃ is tetragonal rather than cubic cannot explain such a large discrepancy. Another possible explanation will be discussed below.

It should be kept in mind that the present results refer to heterojunctions formed by cubic crystals. We deliberately neglected possible distortions of the perovskite structure, which can obviously affect the heterojunction energy band diagram. The point is that the question about the character of these distortions is not so simple as it can seem first. It is known that the character of distortions in these compounds can vary strongly under the biaxial strain, and distortions in two materials are usually tightly coupled with each other. These effects are well known in ferroelectric superlattices [33, 40–42]. In the case of heterojunctions that include polar materials, the necessity of satisfying the

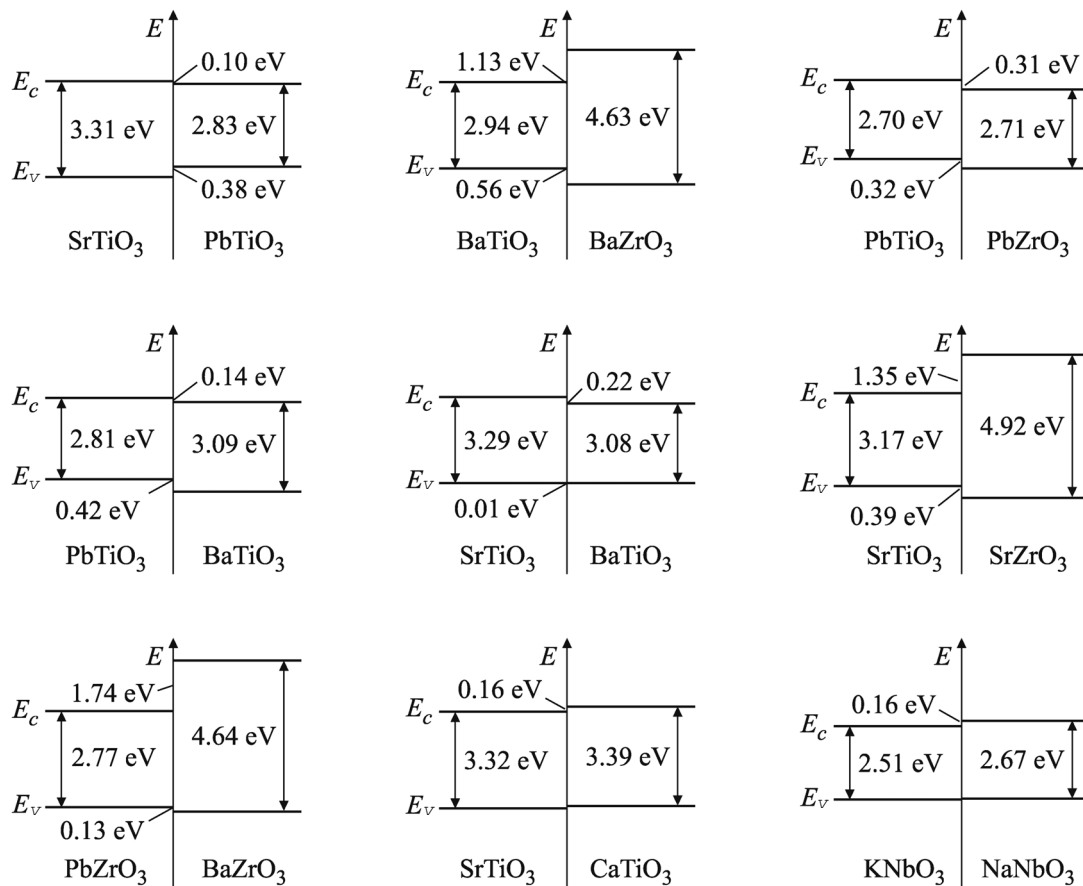


Fig. 4. Energy band diagrams of all heterojunctions studied in this work.

electrical boundary conditions (the equality of the electric displacement field components normal to the interface) results in that the polarization in each of contacting materials differs from the equilibrium polarization. Since the atomic displacements affect the band gap and the band edge positions, the band offsets in polar heterojunctions can be very different from those in nonpolar structures.³ Moreover, cases are known where even a periodic domain structure can appear in a ferroelectric near the interface [43]. It is especially difficult to predict the energy band diagram for such a system.

If the interface is not perfect (e.g., in the case of structural relaxation of strained materials as occurred in [27, 29]), the dangling bonds are formed at the interface, and the surface states appear in the electronic structure. These states are electrically active and can alter substantially ΔV , and so can affect ΔE_c and ΔE_v . In addition, an extra drift of E_v and E_c (the band bending) can occur in the relaxation region in which the lattice parameter depends on the coordinate. The

energy band diagram distortions similar to those caused by surface states can also appear in heterojunctions between strongly defective materials. Like the surface states, defects in contacting materials can exchange electrons with each other; this will distort the heterojunction energy band diagram. In this case, the sizes of the regions in which this exchange occurs can be rather small. For example, the impurity screening radius can be as small as 43 Å at the defect density of 10^{18} cm^{-3} [44]. It is possible that the above-discussed large discrepancy between calculations and experiment for the SrTiO₃/PbTiO₃ heterojunction is due to defects in materials: the band offsets observed in this heterojunction correspond exactly to the case when the levels of defects in two materials are close in energy. In the case of heterojunctions formed by a pair of perovskites with the “valence discontinuity” such as SrTiO₃/LaAlO₃ [28] or BiFeO₃/SrTiO₃ [29], the energy band diagram can be additionally altered by the appearance of quasi-two-dimensional electron gas at the interface.

Finally, we discuss the applicability of the transitivity rule which is often used to calculate the band offsets in heterojunctions by comparing the band offsets for a pair of heterojunctions formed by the components of

³ The same reasoning is also applicable to semiconductor heterojunctions such as GaN/AlN with the wurtzite structure, in which contacting materials have nonzero spontaneous polarization.

the heterojunction under study with a third common component (see, e.g., [26, 45]).

The application of the calculated band offsets ΔE_v to closed chains $\text{SrTiO}_3/\text{PbTiO}_3/\text{BaTiO}_3/\text{SrTiO}_3$, $\text{BaTiO}_3/\text{PbTiO}_3/\text{PbZrO}_3/\text{BaZrO}_3/\text{BaTiO}_3$, and $\text{SrTiO}_3/\text{PbTiO}_3/\text{PbZrO}_3/\text{BaZrO}_3/\text{BaTiO}_3/\text{SrTiO}_3$ to test the transitivity rule shows that we never obtain zero by contour traversing; the deviation is from -0.027 to $+0.539$ eV. Such a behavior is caused by the dependence of the band offsets on the in-plane lattice parameter in a heterojunction [25, 30, 37, 39]. If the lattice parameter would be identical for all heterojunctions entering the chain, the contour traversing would yield zero.⁴ However, since the lattice parameter is different for all heterojunctions entering the chains, the result is nonzero. Thus, the transitivity rule appears inapplicable in the general case, and the error can exceed 0.5 eV.

6. CONCLUSIONS

The band offsets for nine heterojunctions formed by titanates, zirconates, and niobates with the cubic perovskite structure were calculated from first principles. The effect of strain in contacting oxides on their energy structure; the GW corrections to the band edge positions resulting from the many-body effects; and the conduction band edge splitting resulting from spin-orbit coupling were consistently taken into account. It was shown that the neglect of the many-body effects can cause errors in the determination of the band offsets, reaching 0.36 eV. The fundamental inapplicability of the transitivity rule which is often used to determine the band offsets in heterojunctions was demonstrated. The cause of this inapplicability is the dependence of the band offsets on the in-plane lattice parameter in a heterojunction.

The calculations presented in this work were performed on the laboratory computer cluster and the SKIF-MGU “Chebyshev” supercomputer.

ACKNOWLEDGMENTS

This work was supported by the Russian Foundation for Basic Research (project no. 13-02-00724).

REFERENCES

1. A. Ohtomo and H. Y. Hwang, *Nature (London)* **427**, 423 (2004).
2. A. Brinkman, M. Huijben, M. van Zalk, J. Huijben, U. Zeitler, J. C. Maan, W. G. van der Wiel, G. Rijnders, D. H. A. Blank, and H. Hilgenkamp, *Nat. Mater.* **6**, 493 (2007).
3. N. Reyren, S. Thiel, A. D. Caviglia, L. F. Kourkoutis, G. Hammerl, C. Richter, C. W. Schneider, T. Kopp, A.-S. Rüetschi, D. Jaccard, M. Gabay, D. A. Muller, J.-M. Triscone, and J. Mannhart, *Science (Washington)* **317**, 1196 (2007).
4. A. D. Caviglia, S. Gariglio, N. Reyren, D. Jaccard, T. Schneider, M. Gabay, S. Thiel, G. Hammerl, J. Mannhart, and J.-M. Triscone, *Nature (London)* **456**, 624 (2008).
5. S. Thiel, G. Hammerl, A. Schmehl, C. W. Schneider, and J. Mannhart, *Science (Washington)* **313**, 1942 (2006).
6. C. Cen, S. Thiel, G. Hammerl, C. W. Schneider, K. E. Andersen, C. S. Hellberg, J. Mannhart, and J. Levy, *Nat. Mater.* **7**, 298 (2008).
7. C. H. Ahn, S. Gariglio, P. Paruch, T. Tybell, L. Antognazza, and J.-M. Triscone, *Science (Washington)* **284**, 1152 (1999).
8. X. Hong, A. Posadas, A. Lin, and C. H. Ahn, *Phys. Rev. B: Condens. Matter* **68**, 134415 (2003).
9. T. Kanki, H. Tanaka, and T. Kawai. *Appl. Phys. Lett.* **89**, 242506 (2006).
10. H. J. A. Molegraaf, J. Hoffman, C. A. F. Vaz, S. Gariglio, D. van der Marel, C. H. Ahn, and J.-M. Triscone, *Adv. Mater. (Weinheim)* **21**, 3470 (2009).
11. J. Mannhart and D. G. Schlom, *Science (Washington)* **327**, 1607 (2010).
12. P. Zubko, S. Gariglio, M. Gabay, P. Ghosez, and J.-M. Triscone, *Annu. Rev. Condens. Matter Phys.* **2**, 141 (2011).
13. H. Y. Hwang, Y. Iwasa, M. Kawasaki, B. Keimer, N. Nagaosa, and Y. Tokura, *Nat. Mater.* **11**, 103 (2012).
14. T. Choi, S. Lee, Y. J. Choi, V. Kiryukhin, and S.-W. Cheong, *Science (Washington)* **324**, 63 (2009).
15. C. Wang, K. Juan Jin, Z. Tang Xu, L. Wang, C. Ge, H. Bin Lu, H. Zhong Guo, M. He, and G. Zhen Yang, *Appl. Phys. Lett.* **98**, 192901 (2011).
16. M. Y. Zhuravlev, R. F. Sabirianov, S. S. Jaswal, and E. Y. Tsybal, *Phys. Rev. Lett.* **94**, 246802 (2005).
17. H. Kohlstedt, N. A. Pertsev, J. Rodríguez Contreras, and R. Waser, *Phys. Rev. B: Condens. Matter* **72**, 125341 (2005).
18. V. Garcia, S. Fusil, K. Bouzehouane, S. Enouz-Védrenne, N. D. Mathur, A. Barthélémy, and M. Bibes, *Nature (London)* **460**, 81 (2009).
19. J. Padilla, W. Zhong, and D. Vanderbilt, *Phys. Rev. B: Condens. Matter* **53**, R5969 (1996).
20. B. Meyer and D. Vanderbilt, *Phys. Rev. B: Condens. Matter* **65**, 104111 (2002).
21. J. Junquera and P. Ghosez, *Nature (London)* **422**, 506 (2003).
22. N. Sai, A. M. Kolpak, and A. M. Rappe, *Phys. Rev. B: Condens. Matter* **72**, 020101 (2005).
23. S. A. Chambers, Y. Liang, Z. Yu, R. Droopad, and J. Ramdani, *J. Vac. Sci. Technol. A* **19**, 934 (2001).
24. F. Amy, A. S. Wan, A. Kahn, F. J. Walker, and R. A. McKee, *J. Appl. Phys.* **96**, 1635 (2004).
25. J. Junquera, M. Zimmer, P. Ordejón, and P. Ghosez, *Phys. Rev. B: Condens. Matter* **67**, 155327 (2003).
26. R. Schafrank, S. Li, F. Chen, W. Wu, and A. Klein, *Phys. Rev. B: Condens. Matter* **84**, 045317 (2011).

⁴This is indeed observed for a set of three almost isoperiodic heterojunction pairs Ge/GaAs , Ge/ZnSe , and GaAs/ZnSe [45].

27. R. Schafranek, J. D. Baniecki, M. Ishii, Y. Kotaka, K. Yamanka, and K. Kurihara, *J. Phys. D: Appl. Phys.* **45**, 055303 (2012).
28. L. Qiao, T. C. Droubay, V. Shutthanandan, Z. Zhu, P. V. Sushko, and S. A. Chambers, *J. Phys.: Condens. Matter* **22**, 312201 (2010).
29. R. Schafranek, J. D. Baniecki, M. Ishii, Y. Kotaka, and K. Kurihara, *New J. Phys.* **15**, 053014 (2013).
30. L. Colombo, R. Resta, and S. Baroni, *Phys. Rev. B: Condens. Matter* **44**, 5572 (1991).
31. A. Baldereschi, S. Baroni, and R. Resta, *Phys. Rev. Lett.* **61**, 734 (1988).
32. A. I. Lebedev, *Phys. Solid State* **51** (2), 362 (2009).
33. A. I. Lebedev, *Phys. Solid State* **52** (7), 1448 (2010).
34. G. Onida, L. Reining, and A. Rubio, *Rev. Mod. Phys.* **74**, 601 (2002).
35. F. Bruneval and X. Gonze, *Phys. Rev. B: Condens. Matter* **78**, 085125 (2008).
36. C. Hartwigsen, S. Goedecker, and J. Hutter, *Phys. Rev. B: Condens. Matter* **58**, 3641 (1998).
37. C. G. Van de Walle and R. M. Martin, *Phys. Rev. B: Condens. Matter* **34**, 5621 (1986).
38. R. Shaltaf, G.-M. Rignanese, X. Gonze, F. Giustino, and A. Pasquarello, *Phys. Rev. Lett.* **100**, 186401 (2008).
39. D. Cociorva, W. G. Aulbur, and J. W. Wilkins, *Solid State Commun.* **124**, 63 (2002).
40. K. Johnston, X. Huang, J. B. Neaton, and K. M. Rabe, *Phys. Rev. B: Condens. Matter* **71**, 100103 (2005).
41. L. Kim, J. Kim, U. V. Waghmare, D. Jung, and J. Lee, *Phys. Rev. B: Condens. Matter* **72**, 214121 (2005).
42. A. I. Lebedev, *Phys. Solid State* **51** (11), 2324 (2009).
43. E. Bousquet, J. Junquera, and P. Ghosez, *Phys. Rev. B: Condens. Matter* **82**, 045426 (2010).
44. L. M. Falicov and M. Cuevas, *Phys. Rev.* **164**, 1025 (1967).
45. H. Kroemer, in *Molecular Beam Epitaxy and Heterostructures*, Ed. by L. L. Cheng and K. Ploog (M. Nijhoff, Dordrecht, The Netherlands, 1985), p. 331.

Translated by A. Kazantsev